Effects of Chemical Feedbacks on Decadal Methane Emissions Estimates

Newton H. Nguyen[1], Alexander J. Turner[2,3,4], Yi Yin[1], Michael J. Prather[5], Christian Frankenberg[1,4]

[1]Division of Geological and Planetary Sciences, California Institute of Technology, Pasadena, CA, 91125, USA

[2]Department of Earth and Planetary Sciences, University of California, Berkeley, Berkeley, CA, 94720, USA

[3]College of Chemistry, University of California, Berkeley, Berkeley, CA, 94720, USA

[4]NASA Jet Propulsion Lab, California Institute of Technology, Pasadena, CA, 91109, USA

[5]Department of Earth System Science, University of California, Irvine, Irvine, CA, 92697, USA

Key Points:

- Neglecting chemical feedbacks can bias estimates of methane emissions perturbations by up to 25% over 10 years
- Strong biomass burning events, such as El Niño, can indirectly increase the methane growth rate through emission of CO by extending the methane lifetime
- Attributions of decadal trends in methane are dependent on the assumptions about both OH and CO

Corresponding author: Newton Nguyen, `newton@caltech.edu`

Corresponding author: Christian Frankenberg, `cfranken@caltech.edu`

–1–

Abstract

The coupled chemistry of carbon monoxide (CO), methane and hydroxyl radical (OH) can modulate methane's 9-year lifetime, often being ignored in methane-flux inversions, and the impacts of neglecting those feedbacks have not been quantified. Using a coupled-chemistry box model, we show that neglecting methane's effect on [OH] can lead to a 25% bias in calculating methane source perturbations after only 10 yr. Further, CO, such as from biomass burning, can have a comparable impact on methane concentrations as direct-methane emissions, yet acting at much larger spatial scales and delayed by several months. Finally, we quantify the biases of including (or excluding) coupled chemistry in the context of recent methane and CO trends. Inter-annual variations and decreasing trends in CO concentrations have substantial impacts on-methane flux inversions. Given these non-negligible errors, decadal-methane-emissions inversions should incorporate chemical feedbacks for more robust methane trend analyses and source attributions.

Plain Language Summary

Methane inversion studies commonly assume that atmospheric methane has a 9-year lifetime, but the decay rate of methane perturbations can be extended by 40%. This effect is from interactions of other atmospheric compounds with methane's main sink, the hydroxyl radical. This is important for estimating global emissions over recent decades. We show that one of these compounds, carbon monoxide (CO), emitted from wildfires during El Niño, can lead to large increases in methane concentrations by extending the methane lifetime. Moreover, ignoring these effects can lead up to a 25% error in estimating methane emissions changes after a decade. Finally, we show that the effect of decreasing CO on methane has extended the methane lifetime and has led to some biases in calculating methane emissions. Thus, attributing causes of recent methane emissions trends are dependent on the consideration of compounds indirectly affecting the methane lifetime, which may have implications for future mitigation plans.

1 Introduction

Methane is the second most important anthropogenic greenhouse gas. Globally averaged concentrations have risen from $\sim$750 ppb during the pre-industrial to 1850 ppb in 2018, contributing to $\sim$25% of overall radiative forcing (IPCC, 2013), with even higher contributions when considering all indirect impacts (Shindell et al., 2005). This increase includes a brief pause from 2000 to 2007 with a subsequent resumption in growth. The cause of the onset and termination of this stabilization remains debated (see Turner et al., 2019, and references therein for a review of recent trends). Due to nonlinear feedbacks affecting the main methane sink, which is oxidation by the Hydroxyl Radical (OH), perturbations of methane and other species controlling OH loss may affect the methane lifetime (Prather, 1994, 1996), especially in the context of recent methane and CO trends. This is often overlooked in methane inversion studies, as static OH fields are often employed, which may impact flux inversions at longer time-scales (Prather & Holmes, 2017). Our main objective here is to investigate how assumptions on the oxidant chemistry affect methane emissions estimates.

Variations in methane fluxes have been inferred with constraints from methane concentrations and δ^{13}C growth rates to study the 2000-2007 stabilization. However, by ignoring coupled chemistry, there are no changes in methane loss, thus any changes in methane abundances can only be attributed to methane source changes (e.g., Nisbet et al., 2016; Schaefer et al., 2016; Schwietzke et al., 2016; Thompson et al., 2018; J. Worden et al., 2017).

Other studies have focused on a possible change in the main methane sink (e.g., Gaubert et al., 2017; McNorton et al., 2016; Rigby et al., 2017; Turner et al., 2017). Gaubert et al. (2017) focused on the impact of CO on the methane lifetime. They found that a decline in CO concentrations, resulting from decreases in CO emissions in the 2000s (H. Worden et al., 2013), would result in increased OH concentrations during the stabilization period and, consequently, a decline in the methane lifetime. This change in the methane lifetime would require an even stronger increase in methane emissions to explain recent trends.

Rigby et al. (2017) and Turner et al. (2017) concluded it was likely that OH concentrations declined during the stabilization period. However, both studies ignored interactive chemistry but used observations of methyl chloroform (MCF) to constrain globally averaged OH concentrations. Yet, Prather and Holmes (2017) pointed out two main problems: 1), using MCF to constrain OH is highly uncertain due to uncertainties in MCF emissions and loss, and 2) both studies did not explicitly account for chemical feedbacks (terms beyond the first order terms in Eq. 1). Given these uncertainties, alongside the contradicting hypotheses discussed here, the question remains: *"how do simplifying assumptions on coupled chemistry affect methane emissions estimates?"*

Studies employ simplifying assumptions in order to decrease computational cost, and the biases inherent in those assumptions are not well characterized, possibly contributing to contradicting hypotheses around the stabilization period. For instance, box model results have been criticized for not realistically modeling the impacts of atmospheric transport (Naus et al., 2019). On the other hand, sophisticated atmospheric transport models with 3D chemistry are used to invert methane fluxes, but they typically use static OH fields to model methane oxidation. In that context, we believe that the simplicity of a box model is an ideal way to isolate the impact of neglecting coupled chemistry on methane flux inversions from other error sources. To do this, we can conceptualize the complexity of the coupled drivers affecting the decay of a methane perturbation $\delta[\mathrm{CH_4}]$ into a linear expansion of chemical mechanisms, similar to Taylor Series expansions:

$$\frac{d\delta[\mathrm{CH_4}]}{dt} = \sum_i \left(\frac{\partial(d[\mathrm{CH_4}]/dt)}{\partial[X_i]} \right) \delta[X_i]. \tag{1}$$

In Eq. 1, each X_i represents the concentration of species i (e.g. methane, CO, OH, NO_x), which might interact with the methane lifetime. Conceptually, a perturbation in i will either directly affect the methane lifetime (as is the case for [OH]) or indirectly affect methane loss by changing oxidant levels (e.g., higher CO will lead to a decrease in OH, whereas NO_x emissions will typically lead to increased OH abundance and methane loss). The coupled chemistry comes into play as methane oxidation impacts the steady state concentration of OH itself directly and indirectly, as the oxidation leads to CO, which interacts with OH at shorter timescales. Here, we focus on the coupled chemistry of methane, CO, and OH by using a 2-hemispheres box model with coupled methane, CO, and OH chemistry (Prather, 1994, 1996). We will quantify the impacts of critical assumptions in methane flux inversions (Table 1).

2 Forward Model and Variable Lifetimes

2.1 Constructing the Forward Model

OH oxidizes methane to form CO, which is also oxidized by OH, resulting in a coupled chemical system (Table A1). The equations in Table A1 are solved for each hemispheric box. The exchange between the hemispheric boxes are a function of the inter-hemispheric exchange time (1 yr) and inter-hemispheric concentration gradients.

We also employ simplifying assumptions to our model to abstract the complexity of OH production, recycling, and loss. OH is also the primary oxidant for a number of

other compounds in the atmosphere (e.g., ethane and other non-methane hydrocarbons) (Lelieveld et al., 2016), so we follow Prather (1994, 1996) and abstract this complexity with an arbitrary molecule, X, acting as an additional OH sink. In TAble 1 and A1, S_{OH} represents the production rate of OH, which is primarily driven by UV radiation in the presence of ozone and water vapor, in addition to chemical recycling by other species, especially NO_x (Lelieveld et al., 2002, 2016; Nicely et al., 2018). We do not explicitly account for these effects here and instead abstract this complexity with a term, S_{OH}, in our model, which then yields the OH concentration given the sources and sinks of OH. It should also be noted that here, non-interactive chemistry means that the methane oxidation rate is static, meaning that the globally averaged methane lifetime as well as the perturbation decay rates are fixed to ∼9 yr. On the other hand, interactive chemistry allows for [OH] to respond to changes in CO and CH_4, even if S_{OH} is constant.

Direct measurements of OH are neither spatially dense enough, nor sufficiently precise to estimate global mean OH concentrations. This is because OH has a short lifetime (∼1 seconds), exists in low concentrations ($\sim 10^6$ molecules/cm^3), and have large variations in space and time, so variations in MCF are often used as a proxy for globally integrated OH concentrations (e.g., Bousquet et al., 2005; Montzka et al., 2011).

2.2 Chemical Feedbacks Result in Extended Methane Lifetime

Perturbations to methane do not decay with the methane budget lifetime, which is obtained by dividing the total atmospheric methane burden with the methane loss rate assuming steady-state. Instead, in order to account for the nonlinearities in the methane-CO-OH system, perturbation decay rates are calculated from eigenvalues of the Jacobian of the chemical system, (Prather, 1994, 1996; Holmes, 2018).

$$\mathbf{M}_{ij} = \frac{\partial(d[\mathrm{x_i}]/dt)}{\partial[\mathrm{x_j}]}. \tag{2}$$

Each element of the Jacobian, $\mathbf{M}$, consists of the derivative of the rate equations in Table A1, $(d[\mathrm{x_i}]/dt)$, with respect to each species, $[\mathrm{x}_j]$. The complexity of the system is caused by the off-diagonal elements in the matrix, resulting in different perturbation modes with respective decay rates. This perturbation decay rate is also a function of the concentrations of the species in $\mathbf{M}$, because the eigenvalues depend on the values in $\mathbf{M}$. Substituting methane, CO, and OH concentrations of the modern atmosphere into Eq. 2 and inverting the minimum eigenvalue of $\mathbf{M}$ results in the methane perturbation lifetime that is ∼40% longer than the budget lifetime.

We demonstrate this extended perturbation lifetime in Fig. 1A, running the model with prescribed emissions, adding a 10 Tg perturbation to methane emissions with interactive and non-interactive chemistry Fig. 1A. The perturbation lifetime of the non-interactive chemistry model decays with a ∼9.4 yr e-folding lifetime, while the interactive chemistry decays with a ∼13.2 yr lifetime. This is expected (Prather, 1994, 1996) and indicates that our forward box model is a realistic approximation of the chemical system. It should be noted that this perturbation lifetime also holds for infinitesimally small perturbations to methane or CO, which drive correspondingly small perturbations to OH, a fact that is sometimes overlooked. The question is what impact these differences have on decadal-scale flux inversions, because most studies assume a fixed ∼9 yr lifetime. As can be seen in Figure 1a, a methane perturbation decays much slower, so we expect an overestimation of methane flux inversions if this effect is ignored.

Chemical simulations of interactive chemistry, when compared to non-interactive chemistry, result in different equilibrium methane concentrations. We demonstrate this in Fig. 1b, where methane emissions are fixed to 275, 550, 1100, and 2200 Tg/yr with both interactive (solid lines) and non-interactive (dashed lines) chemistry. For emissions larger than the contemporary 550 Tg/yr case (Saunois et al., 2016), the interactive chem-
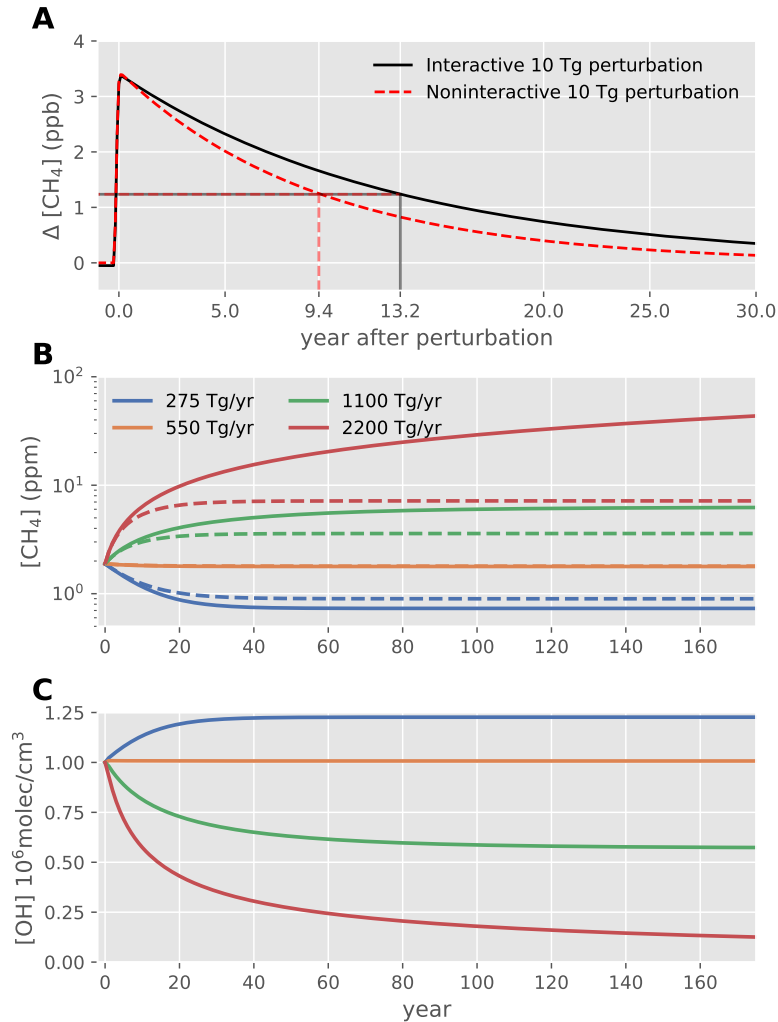
Figure 1. A 10 Tg perturbation of methane (Panel A) decays with a 13.2 yr lifetime for the interactive case (solid line), while the perturbation decays with a 9.4 year lifetime for the non-interactive case (dotted line). Methane concentrations (Panel B) and OH concentrations (Panel C) are shown for our steady-state test, where emissions are fixed to 275, 550, 1100, and 2200 Tg/yr for both interactive (solid lines) and non-interactive (dashed lines) chemistry.

162 istry cases have much higher steady-state methane concentrations than their non-interactive
163 counterparts, because methane concentrations affect OH. However, for the pre-industrial
164 275 Tg/yr case, the interactive steady state concentrations are substantially lower as OH
165 would be about 25% higher. As our prescribed emissions become larger, the difference
166 between methane steady state concentrations in the interactive and non-interactive cases
167 further differ. In the 2200 Tg/yr case, the lifetime and steady-state lifetime differ by more
168 than a factor of three, caused by OH depletion (Fig. 1c). Even after more than 150 years,
169 the 2200 Tg/yr interactive chemistry case reaches concentrations of ∼30 ppm, while OH
170 decreases to 10% of contemporary concentrations, and both have not yet reached a steady
171 state. It should be noted that this simulation ignores other methane sinks, e.g. strato-
172 spheric loss or soil uptake, both of which will dampen this effect in the actual atmosphere
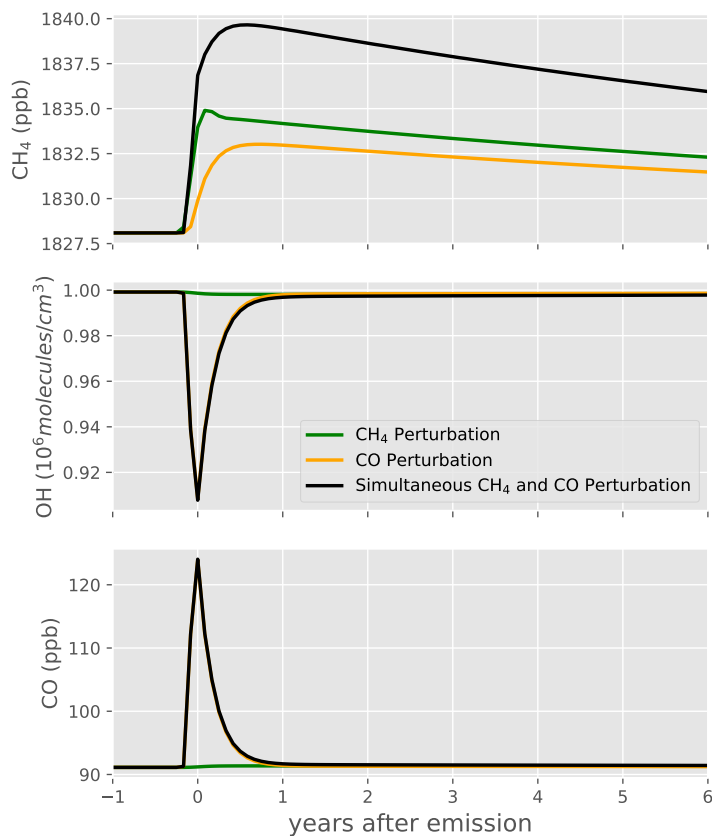173 and avoid a runaway effect.

Figure 2. A 20 Tg pulse of methane (green) increases methane by 6.8 ppb. A 250 Tg perturbation of CO (orange) depletes OH by $\sim -8\%$, extending the methane lifetime, resulting in a 5 ppb increase in methane. The methane and CO joint response (blue) results in a 11.5 ppb increase.

2.3 Effects of El Niño on Methane Concentrations

Here we use the coupled methane-CO-OH chemistry to examine the impact of strong biomass burning during El Niño events on both methane and CO, and consequently OH. Previous works have highlighted the importance of El Niño on methane (e.g., Saunois et al., 2016; J. Worden et al., 2013; Zhang et al., 2018), CO (e.g., Yin et al., 2016), emissions through wetlands and fires. El Niño can further impact OH recycling via changing emissions of lightning NO_x (e.g., Murray et al., 2014; Turner et al., 2018) and through direct NO_x emissions from fires (e.g., Castellanos et al., 2014; Miyazaki et al., 2017), although NO_x effects are not explicitly represented here. However, NO_x emissions will have a more local to regional effect on OH, due to its much shorter lifetime when compared with CO and methane.

Fig. 2 shows the results of three simulations with one-month-long perturbations: 1) a methane release of 20 Tg, 2) a CO release of 250 Tg, and 3) a simultaneous release of 20 Tg methane and 250 Tg CO, which is similar in magnitude to the 1997-1998 El Niño (Randerson et al., 2017). From this, we can observe the response of the system to individual perturbations as well as the joint response, testing our model with other El Niño results (e.g., Butler et al., 2005; Duncan et al., 2003; Rowlinson et al., 2019).

In Fig. 2, methane increases by ∼6.8 ppb to a 20 Tg methane perturbation (the green line) and by ∼5 ppb to the 250 Tg CO perturbation (the orange line). The latter is due to impact of CO on OH concentrations by $\sim -8\%$, not due to direct methane emissions. The decrease in the methane oxidation rate due to the decline in OH increases the methane lifetime in the atmosphere, acting as a pseudo-source of methane that acts over several months even after the fires stopped. This OH response is within the range calculated by other studies using 3-D chemical transport models e.g., Butler et al. (2005) find a $\sim -2.2\%$ decline in [OH] between July 1997 and December 1998 ; Duncan et al. (2003) find -2.2% to -6.8% between September and December 1997 from the Indonesian fires; and most recently, Rowlinson et al. (2019) find $\sim -9\%$ between 1997 and 1998. This indicates that the magnitude of the OH response to CO perturbations in our model is realistic.

The indirect impact through CO emissions is comparable in magnitude to the direct methane emissions, resulting in a much stronger and delayed joint response of methane to perturbations typical for large-scale biomass burning events. The case of the combined methane and CO perturbation results in an 11.5 ppb increase in methane with almost half a year delay in its peak enhancement, demonstrating the coupling of the CH_4-CO-OH system. Hence, it is possible that increases in methane concentrations can be incorrectly attributed to increases in methane emissions, rather than CO emissions (or another species that can impact OH abundances). An El Niño scenario is thus an excellent test case for underlining the importance of interactive chemistry on not only the magnitude of response of methane and [OH] to perturbations, but also the timing of the response. In fact, the impact of biomass burning is highly complex. Locally, direct emissions of methane as well as strong perturbations in NO_x, radiation, CO and other trace gases can play a role, which we cannot quantify in our simplified model. The impact on hemispherically averaged CO concentrations, however, is well captured by our model and has a significant impact on methane concentrations (hence the term pseudo-source) but not in the area of biomass burning directly. Flux inversions using concentration gradients would thus not attribute these background changes in methane concentrations to the actual fires.

3 Inverting for methane Emissions

3.1 Data and Inverse Model

Our box model maps emissions to concentrations and thus, inverting our model maps concentrations to emissions. This enables us to quantify the effects of simplifying assump-

224 tions on methane flux inversions. Emissions are estimated using a non-linear Bayesian
225 inversion method (Rodgers, 2000). We use observations of methane (NOAA), CO (NOAA),
226 and MCF (NOAA, GAGE/AGAGE) concentrations, where hemispherically averaged ob-
227 servations were computed following the methods in Turner et al. (2017). Please refer to
228 Sec Appendix B for more details on averaging methods and stations selected.

3.2 Inversion Bias without Interactive OH Chemistry

230 Here we estimate the impact of neglecting interactive OH chemistry in an ideal-
231 ized inversion test case. Methane emissions are prescribed in our forward model, assum-
232 ing interactive chemistry with a constant 6300 Tg/yr-OH source, resulting in a synthetic
233 methane concentrations time-series, shown in Fig. 3A. We use a scenario in which methane
234 emissions abruptly and permanently increase from 550 to 570 Tg/yr, an increase sim-
235 ilar to the one needed to explain the renewed growth rate after 2007. The resulting syn-
236 thetic concentrations in Fig. 3A constitute synthetic observations used in two inversions,
237 where we assume A) non interactive chemistry, and B) interactive chemistry. This test
238 serves two purposes: 1) to test the performance of our inversion, and 2) to calculate the
239 error associated with neglecting interactive OH chemistry in an inversion, as was alluded
240 to in (Prather & Holmes, 2017). This is equivalent to computing the forward model er-
241 ror of assuming fixed OH concentrations in atmospheric methane inversions (while the
242 true atmosphere is interactive).

243 From our synthetic emissions test results (Fig. 3B and C), we find that the inver-
244 sion is accurate with interactive chemistry. However, inverted methane emissions, in our
245 non-interactive inversion, are consistently higher after our prescribed emissions increase,
246 (Fig. 3b), reaching an overestimation of about 5 Tg/yr after only 10 years after the emis-
247 sions change, which is 25% of the perturbation. This error increase to well over 8 Tg/yr
248 after more than 20 years. This is because the increased methane emissions decrease OH
249 concentrations, whereas the non-interactive concentrations inversion does not account
250 for this OH response. This is non-negligible, because we only need a 20 Tg/yr source-
251 sink imbalance to explain the 2007 renewed growth. Relative errors in these derived emis-
252 sion trends can thus be considerable if we assume fixed OH concentrations.

3.3 Emissions Estimates with Observed Concentrations

254 We performed inversions with increasing levels of complexity to obtain the biases
255 associated with including (or neglecting) interactive OH chemistry and CO in emissions
256 estimates constrained by methane, CO, and MCF observations. Table 1 describes the
257 assumptions in each experiment. In the non-interactive case (-I), OH concentrations are
258 fixed, and thus, inversions of methane emissions only respond to changes in methane con-
259 centrations, whereas in the interactive case (+I), methane emissions adjust to changes
260 in both methane and OH concentrations. In particular, the $\sim$210 ppb increase of methane
261 between 1984 and 2017 would, assuming a constant OH source, decrease OH abundances
262 by $\sim$3.5%, extending the methane lifetime and result in an overestimation of methane
263 emissions when compared to a scenario where [OH] is held constant (-I). The blue line
264 in Fig 4a shows the difference between our methane inversion, which accounts for inter-
265 active chemistry (+I) and non-interactive chemistry (-I). Discounting interactive OH chem-
266 istry would lead to biased trends in the methane fluxes compared to the 1980 baseline,
267 as increasing methane abundances will cause [OH] to decrease. When keeping CO con-
268 stant, this could induce a 20 Tg bias in methane emissions changes between 1980 and 2015,
269 as indicated by the green line's overall declining trend between 1980 and 2017.

270 Accounting for the decrease in CO emissions (Fig. 4d) would increase the avail-
271 ability of OH radicals to oxidize methane. We quantify this impact ($+I/+S_{CO}$) by al-
272 lowing our inversion to adjust to the declining CO concentrations (Fig. 4d), fitting for
273 CO sources, and comparing this to our non-interactive OH inversion (-I). CO sources ex-
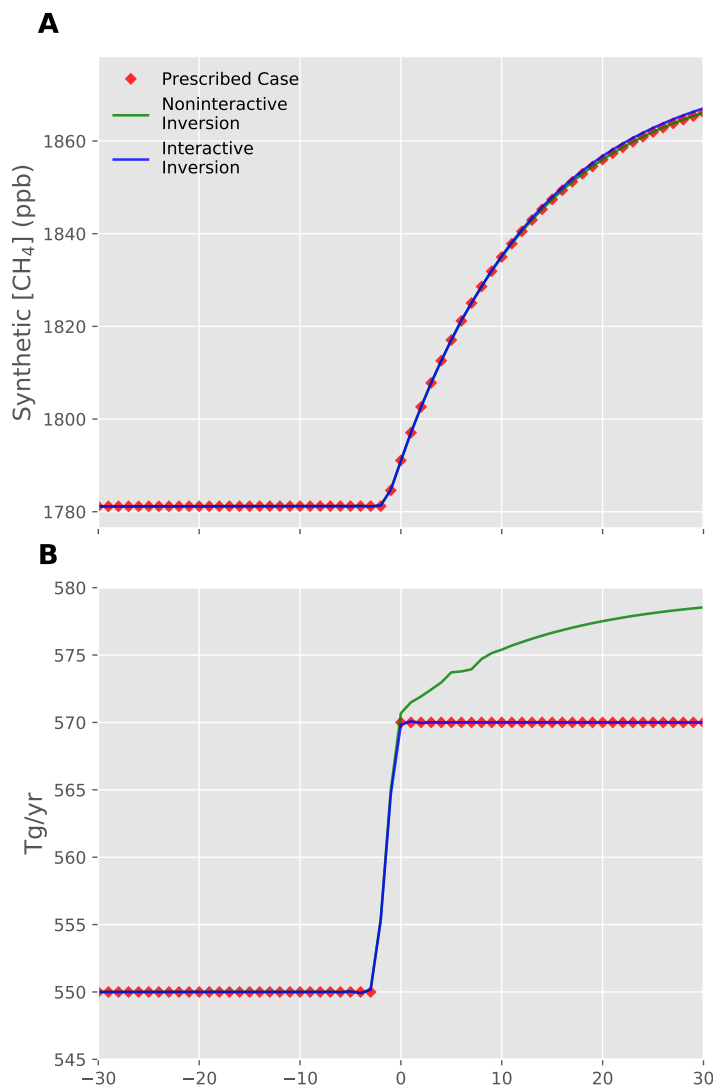
Figure 3. Inversion with prescribed emissions: Methane emissions were prescribed with an abrupt +20 Tg/yr step-change in emissions, resulting in a time-series of methane concentrations (shown in red in Panel A). These synthetic observations were used in two inversions shown in Panel B: Interactive OH Inversion (blue line) and Non-interactive OH Inversion (green line). Note that the prescribed emissions are shown as red diamonds in Panel B but are difficult to see, as they overlap with the Interactive OH Inversion.

Table 1. Varying complexity of simulations for flux inversions corresponding to experiments in Fig. 4.

Case Label	Interactive OH	Inverting [OH]	Inverting S_{CO}	Inverting S_{OH}	Constrained by
$-I$	no	no	n/a	n/a	$[CH_4]$
$-I + [OH]$	no	yes	n/a	n/a	$[CH_4][MCF]$
$+I$	yes	n/a	no	no	$[CH_4][MCF]$
$+I + S_{CO}$	yes	n/a	yes	no	$[CH_4][MCF][CO]$
$+I + S_{OH}$	yes	n/a	no	yes	$[CH_4][MCF]$
$+I + S_{CO} + S_{OH}$	yes	n/a	yes	yes	$[CH_4][MCF][CO]$

clude CO from methane oxidation and only considers direct emissions, which include biomass burning and combustion. The orange line's rising slope in Fig. 4a underlines that 1) decreasing CO abundances overcompensate the effect of increasing methane on OH, consistent with Gaubert et al. (2017), and 2) neglecting indirect effects of CO can result in an error of the inter-annual methane source variability of up to 10 Tg/yr. It should be noted here that our interactive chemistry results may differ from more sophisticated chemistry models, because our model only includes methane and CO effects. In reality, the OH source may have regionally increased due to rising NO_x emissions, which would buffer [OH] (Holmes et al., 2013; Naik et al., 2013; Nicely et al., 2018). We do not explicitly include this effect in our model.

Variations in stratospheric ozone and NO_x can result in OH recycling and production variability, and these OH sources have been thought to have increased in recent decades (e.g., Holmes et al., 2013; Naik et al., 2013; Nicely et al., 2018). To quantify this OH-source variability, $(+I + S_{OH})$ incorporates OH source variability, while $(+I + S_{CO} + S_{OH})$ also accounts for CO source variability. When we assume a variable OH source $(+I + S_{OH})$, the variability in methane emissions is dampened, because OH production and recycling are able to compensate for the variability in OH concentrations. As a result, methane emissions stabilize and decline between 2000 and 2010. This result also exhibits similar variability to the case corresponding to Turner et al. (2017) and Rigby et al. (2017), (-I+[OH]), where concentrations are fitted directly, without interactive chemistry. Also fitting for CO emissions $(+I + S_{OH}+S_{CO})$ further dampens the variability of methane emissions, because CO emissions are also allowed to compensate for variability in methane emissions. These cases are also similar to each other until about 2010, when MCF observation uncertainties reach instrument limitations (Naus et al., 2019).

The 1998 peak in methane emissions, due to El Niño, demonstrates the coupling of the methane-CO-OH system. We observe a local maximum in the CO concentrations in 1998 (Fig. 4D). All cases infer an increase in methane emissions with the 1998 El Niño, but the magnitude and duration is markedly different. Specifically, the $(-I)$ case only accounts for methane emissions and infers ∼48 Tg/yr "spike" in 1998 compared to 1997. This methane emissions spike is not observed in the cases with interactive chemistry. This is because they are able to accommodate the 1998 minimum in OH concentrations. As such, the interactive cases find a smaller magnitude emission increase and a different temporal signal. Specifically, 31 Tg/yr for $(+I+S_{OH})$ and 26 Tg/yr for $(+I+S_{OH}+S_{CO})$. When CO sources are also fitted in the latter case, the inversion is allowed to respond to higher CO concentrations (Fig. 4d), and we see even less methane emissions, due to a release of CO from increased biomass burning (Sec. 2.3).
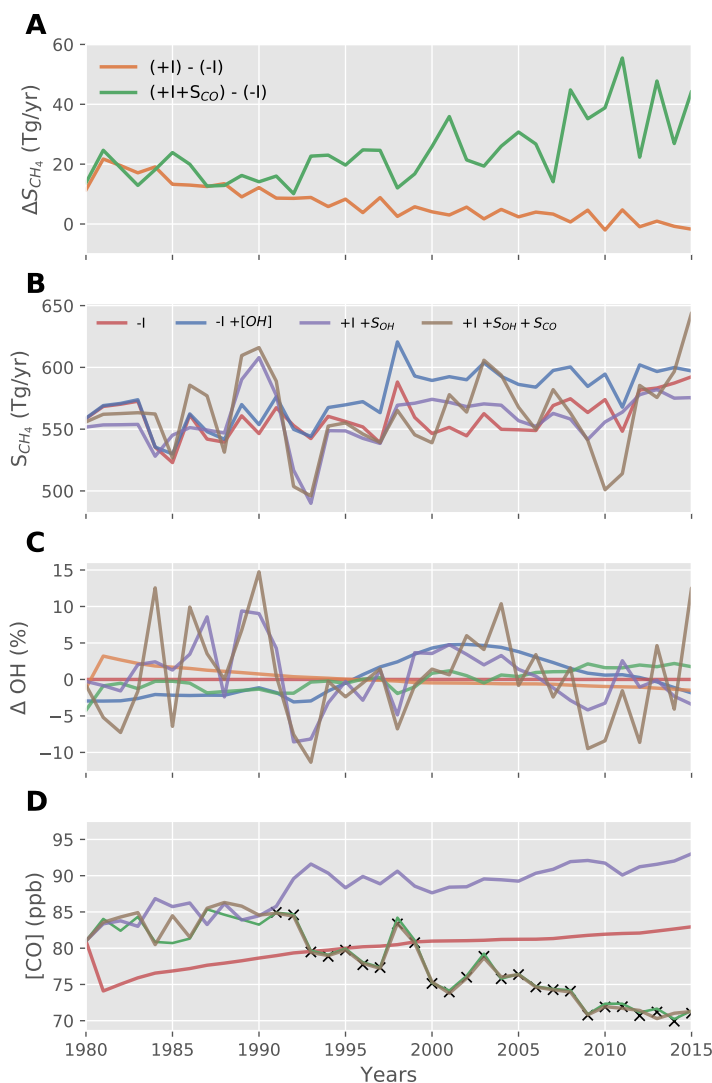
Figure 4. Methane Inversions Constrained by Methane, CO, and MCF Observations: The green line in Panel A shows the difference between our interactive chemistry case (+I) and non-interactive chemistry case (-I), while the orange line shows the difference between our interactive chemistry case with fitted CO sources ($+I + S_{CO}$) and non-interactive chemistry case (-I). Methane emissions calculations (Panel B) differ when the inversion is allowed to respond to variations in OH concentrations (shown in Panel C). Panel D shows observed CO concentrations (black Xes) and our CO fits. The assumptions and constraints for each experiment are listed in Table 1.

4 Summary and Recommendations

Studies calculating global methane emissions have conclusions that are dependent on the assumptions on chemical reaction rates within their inversions. This is because the methane lifetime depends on the concentration of the OH radical which, in turn, depends on the concentration of CO and methane as well as sources of OH. There are no perfect methods to constrain global OH concentrations, and more work should be done to constrain trends in the concentration and production of hydroxyl radicals (e.g., Fortems-Cheiney et al., 2019; Li et al., 2018; Miyazaki et al., 2017; Wolfe et al., 2019). In decadal methane emissions estimates with fixed OH concentrations, we find a systematic and non-negligible negative bias in inversions that do not consider this chemical feedback. When accounting for CO concentration variations, we find decreased CO emissions beginning in the 2000's increased the availability of OH, increasing methane emissions estimates. However, accounting for OH source variability results in methane emissions estimates with similar trend and variability to Rigby et al. (2017) and Turner et al. (2017), where OH concentrations are fitted directly without interactive chemistry. This is due to compensating OH production accounting for variabilities in OH concentrations. It should be noted that other chemical effects that may have a large impact on OH abundances, such as NO_x, Ozone, and water vapor effects (Holmes et al., 2013; Naik et al., 2013; Nicely et al., 2018) are not explicitly represented in our model, so the question *"how does OH production and recycling vary over time?"* remains and should be a priority research objective.

Moving towards a more robust methane trend analysis, global methane emissions inversions at decadal timescales should account for the chemistry affecting methane lifetime in the atmosphere. Inversions with chemical transport models may provide transport effects however, they neglect the non-negligible impacts of OH chemistry on methane lifetime, as their OH fields are usually assumed to be static. This may also have implications for paleoclimate studies (e.g., Dickens et al., 1995; Frieling et al., 2016). Future inversions should include this methane chemical feedback, informed by climate variables relevant for OH production and concentrations. For example, ~90% of variations in OH production can be parameterized by temperature, water vapor, column ozone, biomass burning emissions, and lightning NO_x emissions (Holmes et al., 2013), so OH production and recycling (S_{OH}) can have real-world constraints (Fortems-Cheiney et al., 2019; Castellanos et al., 2014; Holmes et al., 2013; Miyazaki et al., 2017). Simplified parameterizations can capture primary drivers of OH production and recycling, while joint inversions of species that modulate OH concentrations, informed by bottom-up inventories, will more accurately represent methane lifetimes, bringing decadal-scale methane inversions closer to the real world.

Appendix A   2-Hemispheres Box Model

The equations in Table A1 are solved in our 2-hemispheres box model with temperature at $\sim 270°$ K. Interhemispheric transport is dependent on the difference in species concentrations and interhemispheric exchange time (1 yr). We use variations of MCF observations as proxy for global OH variability, which have declined since implementation of the Montreal Protocol Ban (Montzka et al., 2011; Naus et al., 2019). Also note that our box model excludes non-OH sinks, such as loss to the stratosphere, chlorine oxidation, and soil oxidation, and therefore only includes methane and CO loss via OH oxidation. Neglecting these minor processes could alias errors onto our OH concentrations.

Appendix B   Hemispherically Averaged Concentrations

We use observations of methane (NOAA), CO (NOAA), and MCF (NOAA, GAGE/AGAGE) concentrations, where hemispheric averaging was done following Turner et al. (2017). In short, hemispheric averaging was done by bootstrapping from deseasonalized surface observations. We sampled from the observational record in each hemisphere with replacement, where number of times sampled is equal to the number of observational records available in that hemisphere for that species. We also rejected sites that had less than 5 yr of data and required that older observations had higher uncertainties than more recent observations, with a minimum uncertainty of 2 ppb. The randomly drawn observations were blocked-averaged into 1 yr windows. This process was repeated 50 times, so the mean and varience can be computed from these 50 timeseries.

CO is not well-mixed in the atmosphere, exhibiting large spatial gradients. In addition, each species experiences its own oxidative capacities (Naus et al., 2019; Lawrence & Jockel, 2001). Therefore, in order to model CO oxidation by OH, we selected stations in the tropics (23.5° S to 23.5° N). This is because most oxidation of CO occurs in the tropics, where OH concentrations are highest. We refer the reader to Table D1 and D2 for station locations and details. The hemispherically averaged concentrations were calculated with the same bootstrapping procedure outlined above.

Appendix C   OH feedback

In order to obtain the correct perturbation lifetime seen in Fig. 1A, we adjusted the OH source (S_{OH}) and additional loss term ($k_3[x]$). The values we obtained are in Table A1. This results in the 13.2 yr perturbation lifetime.

Appendix D   Bayesian Inversion

We used a non-linear bayesian inversion to obtain the methane fluxes seen in Fig. 3 and 4 (Rodgers, 2000). The elements of the state vector being fitted for are in Table 1 alongside the observations being used to constrain the inversion. The a priori assumptions and prior error for our inversion are shown in Table A1. For the MCF prior in the Northern Hemisphere, we set the error to 20% of the a priori with a minimum of 1.5 Gg. It should also be noted that the temporal correlation we employed was different for the case corresponding to (Rigby et al., 2017) and (Turner et al., 2017) (+I +[OH]) as compared to the other cases, which is the reason why the methane timeseries looks much smoother. We employed much shorter temporal correlations to the other cases in order to make the inter-annual variability more clear.

[ht]

Table A1. The coupled chemical reactions in this table models our simplified chemistry for each hemisphere, denoted by the superscripts.

Chemical Equation	Reaction Constant	a priori emissions	prior error
$\frac{d[CH_4]^N}{dt} = S^N_{CH_4} - k_1^N[CH_4]^N[OH]^N + \frac{[CH_4]^S-[CH_4]^N}{\tau}$	$k_1 = 3.395 \times 10^{-15}\,\frac{cm^3}{molec\;s}$	412.5 Tg/yr	200 Tg
$\frac{d[CH_4]^S}{dt} = S^S_{CH_4} - k_1^S[CH_4]^S[OH]^S + \frac{[CH_4]^N-[CH_4]^S}{\tau}$	$k_1 = 3.395 \times 10^{-15}\,\frac{cm^3}{molec\;s}$	137.5 Tg/yr	200 Tg
$\frac{d[CO]^N}{dt} = S^N_{CO} + k_1[CH_4]^N[OH]^N - k_2[CO]^N[OH]^N + \frac{[CO]^S-[CO]^N}{\tau}$	$k_2 = 1.0133 \times 10^{-12}\,\frac{cm^3}{molec\;s}$	901.5 Tg/yr	800 Tg
$\frac{d[CO]^S}{dt} = S^S_{CO} + k_1[CH_4]^S[OH]^S - k_2[CO]^S[OH]^S + \frac{[CO]^N-[CO]^S}{\tau}$	$k_2 = 1.0133 \times 10^{-12}\,\frac{cm^3}{molec\;s}$	67.5 Tg/yr	56 Tg
$\frac{d[OH]^N}{dt} = S^N_{OH} - k_1[CH_4]^N[OH]^N - k_2[CO]^N[OH]^N - k_3[X]^N[OH]^N$	$k_3[X]^N = 0.99 s^{-1}$	3150 Tg/yr	3150 Tg
$\frac{d[OH]^S}{dt} = S^S_{OH} - k_1[CH_4]^S[OH]^S - k_2[CO]^S[OH]^S - k_3[X]^S[OH]^S$	$k_3[X]^S = 1.23 s^{-1}$	3150 Tg/yr	3150 Tg
$\frac{d[MCF]^N}{dt} = S^N_{MCF} - k_4[MCF]^N[OH]^N + \frac{[MCF]^S-[MCF]^N}{\tau}$	$6.05 \times 10^{-15}\,\frac{cm^3}{molecs}$	238.4 ± 280 Gg/yr	max(1.5, 0.2× (a priori)) Gg
$\frac{d[MCF]^S}{dt} = S^S_{MCF} - k_4[MCF]^S[OH]^S + \frac{[MCF]^N-[MCF]^S}{\tau}$	$6.05 \times 10^{-15}\,\frac{cm^3}{molecs}$	0 Gg/yr	0.5 Gg

Table D1. Monitoring stations used for methane observations.

Station	Code	Latitude	Laboratory
Methane measurements			
Alert, Canada	ALT	82°N	NOAA/ESRL/INSTAAR
Ascension Island, UK	ASC	8°S	NOAA/ESRL/INSTAAR
Terceira Island, Azores	AZR	39°N	NOAA/ESRL/INSTAAR
Baring Head, NZ	BHD	41°S	NOAA/ESRL/INSTAAR
Barrow, USA	BRW	71°N	NOAA/ESRL/INSTAAR
Cold Bay, USA	CBA	55°N	NOAA/ESRL/INSTAAR
Cape Grim, Australia	CGO	41°S	NOAA/ESRL/INSTAAR
Cape Kumukahi, USA	KUM	20°N	NOAA/ESRL/INSTAAR
Lac La Biche, Canada	LLB	55°N	NOAA/ESRL/INSTAAR
High Altitude Global Climate Observation Center, Mexico	MEX	19°N	NOAA/ESRL/INSTAAR
Mace Head, Ireland	MHD	53°N	NOAA/ESRL/INSTAAR
Mauna Loa, USA	MLO	20°N	NOAA/ESRL/INSTAAR
Niwot Ridge, USA	NWR	40°N	NOAA/ESRL/INSTAAR
Cape Matatula, Samoa	SMO	14°S	NOAA/ESRL/INSTAAR
South Pole, Antarctica	SPO	90°S	NOAA/ESRL/INSTAAR
Summit, Greenland	SUM	73°N	NOAA/ESRL/INSTAAR
Tae-ahn Peninsula, Korea	TAP	37°N	NOAA/ESRL/INSTAAR
Mt. Waliguan, China	WLG	36°N	NOAA/ESRL/INSTAAR
Ny-Alesund, Norway	ZEP	80°N	NOAA/ESRL/INSTAAR
Alert, Canada	ALT	82°N	U. Heidelberg
Izana, Portugal	IZA	28°N	U. Heidelberg
Neumayer, Antarctica	NEU	71°S	U. Heidelberg
Niwot Ridge, USA	NWR	41°N	U.C. Irvine
Montana de Oro, USA	MDO	35°N	U.C. Irvine
Cape Grim, Australia	CGO	41°S	U. Washington
Olympic Peninsula, USA	OPW	48°N	U. Washington
Fraserdale, Canada	FSD	50°N	U. Washington
Majuro, Marshall Islands	MMI	7°N	U. Washington
Mauna Loa, USA	MLO	19°N	U. Washington
Baring Head, NZ	BHD	41°S	U. Washington
Barrow, USA	BRW	71°N	U. Washington
Tutuila, Samoa	SMO	14°S	U. Washington

Table D2. Methyl Chloroform and Carbon Monoxide observation stations

Station	Code	Latitude	Laboratory
Methyl Chloroform measurements			
Alert, Canada	ALT	82°N	NOAA/ESRL
Barrow, USA	BRW	71°N	NOAA/ESRL
Cape Grim, Australia	CGO	41°S	NOAA/ESRL
Cape Kumukahi, USA	KUM	20°N	NOAA/ESRL
Mace Head, Ireland	MHD	53°N	NOAA/ESRL
Mauna Loa, USA	MLO	20°N	NOAA/ESRL
Palmer Station, Antarctica	PSA	65°S	NOAA/ESRL
Niwot Ridge, USA	NWR	40°N	NOAA/ESRL
Cape Matatula, Samoa	SMO	14°S	NOAA/ESRL
South Pole, Antarctica	SPO	90°S	NOAA/ESRL
Summit, Greenland	SUM	73°N	NOAA/ESRL
Trinidad Head, USA	THD	41°N	NOAA/ESRL
Cape Grim, Australia	CGO	41°S	GAGE
Mace Head, Ireland	MHD	53°N	GAGE
Cape Meares, USA	ORG	45°N	GAGE
Ragged Point Barbados	RPB	13°N	GAGE
Cape Matatula, Samoa	SMO	14°S	GAGE
Cape Grim, Australia	CGO	41°S	AGAGE
Mace Head, Ireland	MHD	53°N	AGAGE
Ragged Point Barbados	RPB	13°N	AGAGE
Cape Matatula, Samoa	SMO	14°S	AGAGE
Trinidad Head, USA	THD	41°N	AGAGE

Station	Code	Latitude	Laboratory
Carbon Monoxide measurements			
Mauna Loa, USA	MLO	20°N	INSTAAR
Ragged Point Barbados	RPB	13°N	INSTAAR
Cape Matatula, Samoa	SMO	14°S	INSTAAR

References

Bousquet, P., Hauglustaine, D. A., Peylin, P., Carouge, C., & Ciais, P. (2005). Two decades of OH variability as inferred by an inversion of atmospheric transport and chemistry of methyl chloroform. *Atmos. Chem. Phys.*, 22.

Butler, T. M., Rayner, P. J., Simmonds, I., & Lawrence, M. G. (2005). Simultaneous mass balance inverse modeling of methane and carbon monoxide. *Journal of Geophysical Research: Atmospheres*, *110*(D21). Retrieved 2019-11-19, from https://agupubs.onlinelibrary.wiley.com/doi/abs/10.1029/2005JD006071 doi: 10.1029/2005JD006071

Castellanos, P., Boersma, K. F., & van der Werf, G. R. (2014, April). Satellite observations indicate substantial spatiotemporal variability in biomass burning NO$_X$ emission factors for South America. *Atmospheric Chemistry and Physics*, *14*(8), 3929–3943. Retrieved 2019-11-19, from https://www.atmos-chem-phys.net/14/3929/2014/ doi: https://doi.org/10.5194/acp-14-3929-2014

Dickens, G. R., O'Neil, J. R., Rea, D. K., & Owen, R. M. (1995). Dissociation of oceanic methane hydrate as a cause of the carbon isotope excursion at the end of the Paleocene. *Paleoceanography*, *10*(6), 965–971. Retrieved 2019-09-25, from https://agupubs.onlinelibrary.wiley.com/doi/abs/10.1029/95PA02087 doi: 10.1029/95PA02087

Duncan, B. N., Bey, I., Chin, M., Mickley, L. J., Fairlie, T. D., Martin, R. V., & Matsueda, H. (2003). Indonesian wildfires of 1997: Impact on tropospheric chemistry. *Journal of Geophysical Research: Atmospheres*, *108*(D15). Retrieved 2019-11-25, from `https://agupubs.onlinelibrary.wiley.com/doi/abs/10.1029/2002JD003195` doi: 10.1029/2002JD003195

Fortems-Cheiney, A., Pison, I., Dufour, G., Broquet, G., Berchet, A., Potier, E., ... Costantino, L. (2019). Variational regional inverse modeling of reactive species emissions with pyvar-chimere. *Geoscientific Model Development Discussions*, *2019*, 1–22. Retrieved from `https://www.geosci-model-dev-discuss.net/gmd-2019-186/` doi: 10.5194/gmd-2019-186

Frieling, J., Svensen, H. H., Planke, S., Cramwinckel, M. J., Selnes, H., & Sluijs, A. (2016, October). Thermogenic methane release as a cause for the long duration of the PETM. *Proceedings of the National Academy of Sciences*, *113*(43), 12059–12064. Retrieved 2019-09-25, from `https://www.pnas.org/content/113/43/12059` doi: 10.1073/pnas.1603348113

Gaubert, B., Worden, H. M., Arellano, A. F. J., Emmons, L. K., Tilmes, S., Barr, J., ... Edwards, D. P. (2017). Chemical Feedback From Decreasing Carbon Monoxide Emissions. *Geophysical Research Letters*, *44*(19), 9985–9995. Retrieved 2019-01-18, from `https://agupubs.onlinelibrary.wiley.com/doi/abs/10.1002/2017GL074987` doi: 10.1002/2017GL074987

Holmes, C. D. (2018). Methane Feedback on Atmospheric Chemistry: Methods, Models, and Mechanisms. *Journal of Advances in Modeling Earth Systems*, *10*(4), 1087–1099. Retrieved 2019-11-19, from `https://agupubs.onlinelibrary.wiley.com/doi/abs/10.1002/2017MS001196` doi: 10.1002/2017MS001196

Holmes, C. D., Prather, M. J., Svde, O. A., & Myhre, G. (2013, January). Future methane, hydroxyl, and their uncertainties: key climate and emission parameters for future predictions. *Atmospheric Chemistry and Physics*, *13*(1), 285–302. Retrieved 2019-08-19, from `https://www.atmos-chem-phys.net/13/285/2013/` doi: 10.5194/acp-13-285-2013

IPCC. (2013). *Climate Change 2013: The Physical Science Basis. Contribution of Working Group I to the Fifth Assessment Report of the Intergovernmental Panel on Climate Change.* Cambridge, United Kingdom and New York, NY, USA: Cambridge University Press. Retrieved from `www.climatechange2013.org` doi: 10.1017/CBO9781107415324

Lawrence, M. G., & Jockel, P. (2001). What does the global mean OH concentration tell us? *Atmos. Chem. Phys.*, 13.

Lelieveld, J., Gromov, S., Pozzer, A., & Taraborrelli, D. (2016, October). Global tropospheric hydroxyl distribution, budget and reactivity. *Atmospheric Chemistry and Physics*, *16*(19), 12477–12493. Retrieved 2019-03-20, from `https://www.atmos-chem-phys.net/16/12477/2016/` doi: 10.5194/acp-16-12477-2016

Lelieveld, J., Peters, W., Dentener, F. J., & Krol, M. C. (2002, December). Stability of tropospheric hydroxyl chemistry. *Journal of Geophysical Research: Atmospheres*, *107*(D23), ACH 17–1–ACH 17–11. Retrieved 2019-12-31, from `https://agupubs.onlinelibrary.wiley.com/doi/abs/10.1029/2002JD002272` doi: 10.1029/2002JD002272

Li, M., Karu, E., Brenninkmeijer, C., Fischer, H., Lelieveld, J., & Williams, J. (2018, September). Tropospheric OH and stratospheric OH and Cl concentrations determined from CH_4, CH_3Cl, and SF_6 measurements. *npj Climate and Atmospheric Science*, *1*(1), 29. Retrieved 2019-03-20, from `https://www.nature.com/articles/s41612-018-0041-9` doi: 10.1038/s41612-018-0041-9

McNorton, J., Chipperfield, M. P., Gloor, M., Wilson, C., Feng, W., Hayman, G. D., ... Montzka, S. A. (2016, June). Role of OH variability in the stalling of the global atmospheric CH_4 growth rate from 1999 to 2006. *Atmospheric Chemistry and Physics*, *16*(12), 7943–7956. Retrieved 2019-

11-25, from `https://www.atmos-chem-phys.net/16/7943/2016/` doi: https://doi.org/10.5194/acp-16-7943-2016

Miyazaki, K., Eskes, H., Sudo, K., Boersma, K. F., Bowman, K., & Kanaya, Y. (2017, January). Decadal changes in global surface NO_x emissions from multi-constituent satellite data assimilation. *Atmospheric Chemistry and Physics*, *17*(2), 807–837. Retrieved 2019-11-19, from `https://www.atmos-chem-phys.net/17/807/2017/` doi: 10.5194/acp-17-807-2017

Montzka, S. A., Krol, M., Dlugokencky, E., Hall, B., Jckel, P., & Lelieveld, J. (2011, January). Small Interannual Variability of Global Atmospheric Hydroxyl. *Science*, *331*(6013), 67–69. Retrieved 2019-06-19, from `https://science.sciencemag.org/content/331/6013/67` doi: 10.1126/science.1197640

Murray, L. T., Mickley, L. J., Kaplan, J. O., Sofen, E. D., Pfeiffer, M., & Alexander, B. (2014, April). Factors controlling variability in the oxidative capacity of the troposphere since the Last Glacial Maximum. *Atmospheric Chemistry and Physics*, *14*(7), 3589–3622. Retrieved 2019-07-03, from `https://www.atmos-chem-phys.net/14/3589/2014/acp-14-3589-2014.html` doi: https://doi.org/10.5194/acp-14-3589-2014

Naik, V., Voulgarakis, A., Fiore, A. M., Horowitz, L. W., Lamarque, J.-F., Lin, M., … Zeng, G. (2013, May). Preindustrial to present-day changes in tropospheric hydroxyl radical and methane lifetime from the Atmospheric Chemistry and Climate Model Intercomparison Project (ACCMIP). *Atmospheric Chemistry and Physics*, *13*(10), 5277–5298. Retrieved 2019-11-26, from `https://www.atmos-chem-phys.net/13/5277/2013/` doi: 10.5194/acp-13-5277-2013

Naus, S., Montzka, S. A., Pandey, S., Basu, S., Dlugokencky, E. J., & Krol, M. (2019, January). Constraints and biases in a tropospheric two-box model of OH. *Atmospheric Chemistry and Physics*, *19*(1), 407–424. Retrieved 2019-06-07, from `https://www.atmos-chem-phys.net/19/407/2019/` doi: 10.5194/acp-19-407-2019

Nicely, J. M., Canty, T. P., Manyin, M., Oman, L. D., Salawitch, R. J., Steenrod, S. D., … Strode, S. A. (2018). Changes in Global Tropospheric OH Expected as a Result of Climate Change Over the Last Several Decades. *Journal of Geophysical Research: Atmospheres*, *123*(18), 10,774–10,795. Retrieved 2019-06-19, from `https://agupubs.onlinelibrary.wiley.com/doi/abs/10.1029/2018JD028388` doi: 10.1029/2018JD028388

Nisbet, E. G., Dlugokencky, E. J., Manning, M. R., Lowry, D., Fisher, R. E., France, J. L., … Ganesan, A. L. (2016). Rising atmospheric methane: 20072014 growth and isotopic shift. *Global Biogeochemical Cycles*, *30*(9), 1356–1370. Retrieved 2019-11-27, from `https://agupubs.onlinelibrary.wiley.com/doi/abs/10.1002/2016GB005406` doi: 10.1002/2016GB005406

Prather, M. J. (1994, May). Lifetimes and eigenstates in atmospheric chemistry. *Geophysical Research Letters*, *21*(9), 801–804. Retrieved 2019-11-27, from `https://agupubs.onlinelibrary.wiley.com/doi/abs/10.1029/94GL00840` doi: 10.1029/94GL00840

Prather, M. J. (1996, September). Time scales in atmospheric chemistry: Theory, GWPs for CH4 and CO, and runaway growth. *Geophysical Research Letters*, *23*(19), 2597–2600. Retrieved 2018-06-12, from `https://agupubs.onlinelibrary.wiley.com/doi/abs/10.1029/96GL02371` doi: 10.1029/96GL02371

Prather, M. J., & Holmes, C. D. (2017, May). Overexplaining or underexplaining methanes role in climate change. *Proceedings of the National Academy of Sciences*, *114*(21), 5324–5326. Retrieved 2018-06-12, from `http://www.pnas.org/content/114/21/5324` doi: 10.1073/pnas.1704884114

Randerson, J., Van Der Werf, G., Giglio, L., Collatz, G., & Kasibhatla, P. (2017).

Global Fire Emissions Database, Version 4.1 (GFEDv4). ORNL Distributed Active Archive Center. Retrieved from `https://daac.ornl.gov/cgi-bin/dsviewer.pl?ds_id=1293` doi: 10.3334/ORNLDAAC/1293

Rigby, M., Montzka, S. A., Prinn, R. G., White, J. W. C., Young, D., ODoherty, S., ... Park, S. (2017, May). Role of atmospheric oxidation in recent methane growth. *Proceedings of the National Academy of Sciences*, *114*(21), 5373–5377. Retrieved 2018-06-12, from `http://www.pnas.org/content/114/21/5373` doi: 10.1073/pnas.1616426114

Rodgers, C. D. (2000). *Inverse methods for atmospheric sounding: theory and practice* (Vol. 2). World scientific.

Rowlinson, M. J., Rap, A., Arnold, S. R., Pope, R. J., Chipperfield, M. P., McNorton, J., ... Siddans, R. (2019, July). Impact of El NioSouthern Oscillation on the interannual variability of methane and tropospheric ozone. *Atmospheric Chemistry and Physics*, *19*(13), 8669–8686. Retrieved 2019-11-22, from `https://www.atmos-chem-phys.net/19/8669/2019/` doi: https://doi.org/10.5194/acp-19-8669-2019

Saunois, M., Bousquet, P., Poulter, B., Peregon, A., Ciais, P., Canadell, J. G., ... Zhu, Q. (2016, December). The global methane budget 20002012. *Earth System Science Data*, *8*(2), 697–751. Retrieved 2019-11-26, from `https://www.earth-syst-sci-data.net/8/697/2016/` doi: 10.5194/essd-8-697-2016

Schaefer, H., Fletcher, S. E. M., Veidt, C., Lassey, K. R., Brailsford, G. W., Bromley, T. M., ... White, J. W. C. (2016, March). A 21st century shift from fossil-fuel to biogenic methane emissions indicated by 13ch4. *Science*, aad2705. Retrieved 2018-09-11, from `http://science.sciencemag.org/content/early/2016/03/09/science.aad2705` doi: 10.1126/science.aad2705

Schwietzke, S., Sherwood, O. A., Bruhwiler, L. M. P., Miller, J. B., Etiope, G., Dlugokencky, E. J., ... Tans, P. P. (2016, October). Upward revision of global fossil fuel methane emissions based on isotope database. *Nature*, *538*(7623), 88–91. Retrieved 2019-08-19, from `https://www.nature.com/articles/nature19797` doi: 10.1038/nature19797

Shindell, D. T., Faluvegi, G., Bell, N., & Schmidt, G. A. (2005). An emissions-based view of climate forcing by methane and tropospheric ozone. *Geophysical Research Letters*, *32*(4). Retrieved 2019-11-27, from `https://agupubs.onlinelibrary.wiley.com/doi/abs/10.1029/2004GL021900` doi: 10.1029/2004GL021900

Thompson, R. L., Nisbet, E. G., Pisso, I., Stohl, A., Blake, D., Dlugokencky, E. J., ... White, J. W. C. (2018). Variability in Atmospheric Methane From Fossil Fuel and Microbial Sources Over the Last Three Decades. *Geophysical Research Letters*, *45*(20), 11,499–11,508. Retrieved 2019-12-24, from `https://agupubs.onlinelibrary.wiley.com/doi/abs/10.1029/2018GL078127` doi: 10.1029/2018GL078127

Turner, A. J., Frankenberg, C., & Kort, E. A. (2019, February). Interpreting contemporary trends in atmospheric methane. *Proceedings of the National Academy of Sciences*, *116*(8), 2805–2813. Retrieved 2019-06-19, from `https://www.pnas.org/content/116/8/2805` doi: 10.1073/pnas.1814297116

Turner, A. J., Frankenberg, C., Wennberg, P. O., & Jacob, D. J. (2017, April). Ambiguity in the causes for decadal trends in atmospheric methane and hydroxyl. *Proceedings of the National Academy of Sciences*, 201616020. Retrieved 2018-08-14, from `http://www.pnas.org/content/early/2017/04/11/1616020114` doi: 10.1073/pnas.1616020114

Turner, A. J., Fung, I., Naik, V., Horowitz, L. W., & Cohen, R. C. (2018, September). Modulation of hydroxyl variability by ENSO in the absence of external forcing. *Proceedings of the National Academy of Sciences*, *115*(36), 8931–8936. Retrieved 2019-03-20, from `https://www.pnas.org/content/115/36/8931` doi: 10.1073/pnas.1807532115

Wolfe, G. M., Nicely, J. M., Clair, J. M. S., Hanisco, T. F., Liao, J., Oman, L. D., ... Dean-Day, J. (2019, June). Mapping hydroxyl variability throughout the global remote troposphere via synthesis of airborne and satellite formaldehyde observations. *Proceedings of the National Academy of Sciences*, *116*(23), 11171–11180. Retrieved 2019-11-19, from `https://www.pnas.org/content/116/23/11171` doi: 10.1073/pnas.1821661116

Worden, H., Deeter, M. N., Frankenberg, C., George, M., Nichitiu, F., Worden, J., ... Warner, J. X. (2013, January). Decadal record of satellite carbon monoxide observations. *Atmospheric Chemistry and Physics*, *13*(2), 837–850. Retrieved 2019-11-20, from `https://www.atmos-chem-phys.net/13/837/2013/` doi: 10.5194/acp-13-837-2013

Worden, J., Bloom, A. A., Pandey, S., Jiang, Z., Worden, H. M., Walker, T. W., ... Rckmann, T. (2017, December). Reduced biomass burning emissions reconcile conflicting estimates of the post-2006 atmospheric methane budget. *Nature Communications*, *8*(1), 2227. Retrieved 2018-01-18, from `https://www.nature.com/articles/s41467-017-02246-0` doi: 10.1038/s41467-017-02246-0

Worden, J., Jiang, Z., Jones, D. B. A., Alvarado, M., Bowman, K., Frankenberg, C., ... Worden, H. (2013, September). El Nio, the 2006 Indonesian peat fires, and the distribution of atmospheric methane: METHANE FROM 2006 INDONESIAN PEAT FIRES. *Geophysical Research Letters*, *40*(18), 4938–4943. Retrieved 2019-07-02, from `http://doi.wiley.com/10.1002/grl.50937` doi: 10.1002/grl.50937

Yin, Y., Ciais, P., Chevallier, F., Werf, G. R. v. d., Fanin, T., Broquet, G., ... Wang, Y. (2016). Variability of fire carbon emissions in equatorial Asia and its nonlinear sensitivity to El Nio. *Geophysical Research Letters*, *43*(19), 10,472–10,479. Retrieved 2019-11-26, from `https://agupubs.onlinelibrary.wiley.com/doi/abs/10.1002/2016GL070971` doi: 10.1002/2016GL070971

Zhang, Z., Zimmermann, N. E., Calle, L., Hurtt, G., Chatterjee, A., & Poulter, B. (2018, June). Enhanced response of global wetland methane emissions to the 20152016 El Nio-Southern Oscillation event. *Environmental Research Letters*, *13*(7), 074009. Retrieved 2019-07-02, from `https://doi.org/10.1088%2F1748-9326%2Faac939` doi: 10.1088/1748-9326/aac939

Figure 1.

Figure 2.

Figure 4.

Figure 3.